CMS Physics Analysis Summary

Contact: cms-pag-conveners-smp@cern.ch 2014/02/05

Hadronic event shapes in pp collisions at 7 TeV

The CMS Collaboration

Abstract

Event shape variables exhibit sensitivity to the structure of QCD radiation in hadron collisions. Five infrared- and collinear-safe event shape variables, each sensitive to the different features of multi-jet production, are measured using hadronic jet data collected with the CMS detector from pp collisions at $\sqrt{s}$ = 7 TeV, corresponding to a total integrated luminosity of 5 fb^{-1}. The measurements are compared to predictions of various QCD-inspired event generators of multi-jet production.

1 Introduction

Event shape variables are geometric properties of the energy flow in hadronic final states. Many of these are collinear- and infrared-safe, as well as robust with respect to mismeasurement of soft or close-by particles. They are sensitive to the details of the features of quantum chromodynamics (QCD) [1, 2]. They have been extensively studied in earlier electron-positron and deep inelastic lepton-hadron collisions [3–5]. These measurements have improved the understanding of the structure of QCD and have been used for the tuning and validation of various QCD-inspired Monte Carlo (MC) event generators.

In collider experiments, the limited solid angle coverage of the detectors in the longitudinal direction leads to large missing energy. In hadron-hadron collisions this is supplemented with lack of knowledge of the initial momentum of the partonic system, while for e^+e^- collisions the full kinematics can be determined more precisely. This has led to the redefinition of the global event shape variables measured in the transverse plane, where the energy flow can be measured completely and with small systematic uncertainty. A large set of event shape variables has been proposed which are sensitive to different radiation features in proton-proton colliders [1, 2]. These variables are normalized to the sum of the measured transverse momentum of all reconstructed objects in the event to reduce the main systematic uncertainty due to the jet energy scale.

The CDF experiment at the Tevatron [6] has measured event shape variables with unclustered calorimeter cells and compared experimental data with perturbative QCD calculations at next-to-leading order, and with several tunes of the PYTHIA6 event generator [7]. At the LHC, event shape variables have been measured with early data collected in 2010 [8, 9], and recently by the CMS collaboration using associated production of Z + jet events [10].

In the previous analysis [8] by the CMS experiment, the central thrust and thrust minor event shape variables have been used to test various QCD models implemented in MC generators. We continue this study using a larger data set of 5 fb^{-1} and an extended set of event shape variables, which includes transverse thrust, jet broadening, jet mass (both in the transverse plane and in three dimensions), and the three-jet resolution parameter. The latter four observables are analyzed for the first time in CMS. This analysis is sensitive to features of the QCD parton shower that were not probed in the previous analysis.

The paper is organized as follows. In Section 2, elements of the CMS detector relevant to this analysis are described. Section 3 introduces the event shape variables. The data and simulated (MC) event samples used are summarized in Section 4 along with the event selection criteria. Section 5 describes the unfolding technique utilized and the systematic uncertainties. Section 6 presents comparisons between data and several MC models. The results are summarized in Section 7.

2 The CMS Detector

The CMS experiment uses a right-handed coordinate system, with the origin at the nominal interaction point, the x axis pointing to the center of the LHC ring, the y axis pointing vertically up (perpendicular to the plane of the LHC ring), and the z axis along the counterclockwise-beam direction. The polar angle θ is measured from the positive z axis and the azimuthal angle ϕ is measured in the x-y plane. Pseudo-rapidity is defined as $\eta = -\ln[\tan(\theta/2)]$.

The central feature of the CMS detector is a superconducting solenoid, of 6 m internal diameter, providing a field of 3.8 T. Within the field volume, there are a silicon pixel and strip tracker

(TRK), a lead-tungstate crystal electromagnetic calorimeter (ECAL) and a sampling hadron calorimeter (HCAL) made up of layers of brass plates and plastic scintillators. The calorimeters provide coverage in pseudo-rapidity up to $|\eta| < 3.0$. A preshower detector consisting of two planes of silicon sensors interleaved with lead is located in front of the ECAL at $1.653 < |\eta| < 2.6$. An iron and quartz-fiber Cerenkov hadron calorimeter (HF) covers pseudo-rapidities $3.0 < |\eta| < 5.0$. The muons are measured in the pseudo-rapidity range $|\eta| < 2.4$, with detection planes made using three technologies: drift tubes, cathode strip chambers, and resistive plate chambers. Matching the muons to the tracks measured in the silicon tracker results in a transverse momentum resolution between 1 and 5%, for p_{T} values up to 1 TeV. The ECAL has an energy resolution of better than 0.5% for unconverted photons with transverse energies above 100 GeV. A detailed description of the CMS experiment can be found elsewhere [11].

Jets are reconstructed from particle-flow candidates. The particle-flow (PF) algorithm [12, 13] combines information on charged particles from the tracking system, energy deposits in the electromagnetic and hadronic calorimeters, as well as signals in the preshower detector and muon systems to assign the four-momentum vector to particles, *e.g.*, γ, $e^{\pm}$, $\mu^{\pm}$, charged and neutral hadrons. Jets are reconstructed using these particles. Energy calibration of individual particle types is done separately. At this level, the jet constituents are almost fully calibrated and require only a small correction (less than 10%) [14] due to tracking inefficiencies and threshold effects. The jet clustering is performed using the anti-k_{T} clustering algorithm [15, 16] with a distance parameter R = 0.5. The jets are ordered in descending p_{T} with $p_{T,1}$, $p_{T,2}$ representing the transverse momenta of the leading and the second leading jets.

3 Event Shape Variables

Five event shape variables are analyzed in this paper: transverse thrust ($\tau_{\perp,\mathcal{C}}$), total jet broadening parameter ($B_{T,\mathcal{C}}$), total jet mass ($\rho_{Tot,\mathcal{C}}$), total transverse jet mass ($\rho^{T}_{Tot,\mathcal{C}}$) and the third-jet resolution parameter ($y_{23,\mathcal{C}}$). Here in all cases, the symbol $\mathcal{C}$ (central) indicates that the inputs used for evaluation of these variables are the jets in the central region of the detector defined by $|\eta| < 2.4$.

Transverse Thrust: The event thrust observable in the transverse plane is defined by:

$$T_{\perp,\mathcal{C}} \equiv \max_{\hat{n}_T} \frac{\sum_i |\vec{p}_{\perp i} \cdot \hat{n}_T|}{\sum_i p_{\perp i}} , \; \tau_{\perp,\mathcal{C}} \equiv 1 - T_{\perp,\mathcal{C}} , \tag{1}$$

where $\vec{p}_{\perp i}$ represents the transverse momentum of the i-th jet, and $\hat{n}_T$ is the unit vector that maximizes the projection (transverse thrust axis). This variable probes various aspects of QCD radiative processes and is sensitive to the modeling of two-jet and multi-jet topologies. In the limit of a perfectly balanced two-jet event, $\tau_{\perp,\mathcal{C}}$ is zero, while in isotropic multi-jet events it is $(1 - 2/\pi)$.

Jet Broadenings: Having determined the transverse thrust axis $\hat{n}_T$, the transverse region is separated into an upper part $\mathcal{C}_U$, consisting of all jets with $\vec{p}_{\perp} \cdot \hat{n}_T > 0$, and a lower part $\mathcal{C}_L$, with $\vec{p}_{\perp} \cdot \hat{n}_T < 0$. The pseudo-rapidities and the azimuthal angles of the axes for the upper and lower regions are defined by:

$$\eta_X \equiv \frac{\sum_{i \in \mathcal{C}_X} p_{\perp i} \eta_i}{\sum_{i \in \mathcal{C}_X} p_{\perp i}} , \tag{2}$$

$$\phi_X \equiv \frac{\sum_{i \in \mathcal{C}_X} p_{\perp i} \phi_i}{\sum_{i \in \mathcal{C}_X} p_{\perp i}} , \tag{3}$$

where X refers to upper (U) or lower (L) part. The broadening in the two regions are then defined as

$$B_{X,\mathcal{C}} \equiv \frac{1}{2\,P_\perp} \sum_{i \in \mathcal{C}_X} p_{\perp i} \sqrt{(\eta_i - \eta_X)^2 + (\phi_i - \phi_X)^2}\,, \tag{4}$$

where $P_\perp$ is the scalar sum of the transverse momenta of all the jets. The total jet broadening is defined as

$$B_{T,\mathcal{C}} \equiv B_{U,\mathcal{C}} + B_{L,\mathcal{C}}. \tag{5}$$

Jet Masses: For the same definitions of upper and lower regions, the normalized squared invariant mass is defined by:

$$\rho_X \equiv \frac{1}{Q^2} \left(\sum_{i \in \mathcal{C}_X} q_i \right)^2, \tag{6}$$

where Q is the scalar sum of the momenta of all the constituents (q_i) in jets. The jet mass is defined as the sum of the masses in the upper and lower regions,

$$\rho_{Tot,\mathcal{C}} \equiv \rho_U + \rho_L\,. \tag{7}$$

Similarly, the corresponding jet mass in the transverse plane, defined to be the two-dimensional jet mass $\rho^T_{Tot,\mathcal{C}}$, is also calculated.

Jet resolution parameter: The third-jet resolution parameter is defined as

$$y_{23,\mathcal{C}} \equiv \frac{\min(R^2 \times p^2_{T,3},\, \min(p_{T,i}, p_{T,j})^2 \times \Delta R^2_{ij})}{P^2_{12}}\,, \tag{8}$$

where $\Delta R^2_{ij} = (\eta_i - \eta_j)^2 + (\phi_i - \phi_j)^2$, $p_{T,3}$ is the transverse momentum of the third jet in the event, $p_{T,i(j)}$, $\eta_{i(j)}$, and $\phi_{i(j)}$ are the transverse momentum, pseudo-rapidity and azimuthal angle of the $i(j)$-th jet respectively. To compute P_{12}, three jets are merged into two using the k_T-algorithm [17, 18] with a cone-size of R (= 0.6); P_{12} is then defined as the sum of two remaining jets' transverse momenta. If there are more than three jets in the event, they are iteratively merged using the same procedure asabove in order to form two jets.

The $y_{23,\mathcal{C}}$ variable estimates the relative strength of the p_T of the third jet with respect to the other two jets. The $y_{23,\mathcal{C}}$ variable vanishes for two-jet events, and a non-zero value of $y_{23,\mathcal{C}}$ indicates the presence of hard parton emission, which in turn tests the parton showering model of MC generators. This test is less sensitive to the underlying event (UE) or the parton hadronization model than the use of other event shape variables [2].

4 Event Selection and Monte Carlo Samples

In this analysis we extend the phase space with respect to the previous measurements [8] to $|\eta_{jet}| < 2.4$ and consider several different p_T ranges of the leading jet.

This analysis uses events collected with single-jet triggers, where the p_T of at least one jet is above a certain threshold. Events are divided into five bins of $p_{T,1}$ and each bin utilizes data from one trigger path. The choice of ranges of $p_{T,1}$ has been determined by the trigger criteria,

Range of $p_{T,1}$ (GeV/c)	Luminosity (pb^{-1})	Number of events	Fraction of events (%)			
			$N_{jet} = 2$	$N_{jet} = 3$	$N_{jet} = 4$	$N_{jet} > 4$
110 - 170	0.403	96833	57.9	32.6	7.8	1.7
170 - 250	7.15	228854	43.0	37.7	14.6	4.7
250 - 320	153	601554	34.8	37.8	19.1	8.3
320 - 390	521	497827	31.0	37.0	21.2	10.9
> 390	5 fb^{-1}	2234304	28.4	35.6	22.5	13.5

Table 1: Characteristics of data samples selected for this analysis, in categories of leading jet transverse momentum $p_{T,1}$: effective integrated luminosity (pb^{-1}), selected number of events, and relative abundances of the numbers of selected jets N_{jet}, for jets with $p_{T,jet} > 30$ GeV/c and $|\eta_{jet}| < 2.4$.

while the p_{T} threshold for other jets (> 30 GeV/c) and their geometric acceptance ($|\eta| < 2.4$) are restricted to give the best jet energy scale and resolution. Spurious jets due to noise in the calorimeters and other non-collision backgrounds are rejected using jet quality criteria discussed in [8]. An event is discarded if

- any one of the two leading jets lies outside the central region ($|\eta| < 2.4$); note that for the measurement of $B_{T,\mathcal{C}}$ and $y_{23,\mathcal{C}}$, a third jet satisfying the jet selection criteria is required within the same detector acceptance region;
- any one of the two leading jets is spurious;
- all selected jets of an event lie only on one side of the line perpendicular to $\hat{n}_T$. This criterion ensures that events will be rejected if jets in the forward direction are missed. Events of interest for this analysis should be well-balanced in p_{T} and hence have jets on both sides of this line.

Table 1 shows the number of events, as well as the fraction of events with two, three, four, or more than four jets, as a function of $p_{T,1}$ range, along with the total effective integrated luminosity.

Four MC generators, PYTHIA6.426 (PYTHIA6) [7], PYTHIA8.153 (PYTHIA8) [19], HERWIG++ 2.5.0 (HERWIG++) [20] and MADGRAPH 5.1.5.7 (MADGRAPH) [21] were chosen to generate multi-jet events, which are passed through the full CMS detector simulation based on GEANT4 [22]. The simulated events are then reconstructed in the same way as it is done for real data, and they are also used to obtain the unfolding matrix and estimate the associated uncertainties.

The first generator considered is PYTHIA6, with three different tunes: the tune Z2 [23], which uses p_{T}-ordered parton showering (PS) and is based on CMS data collected at 900 GeV and 7 TeV; the PERUGIA-P0 [24] tune, which is based on LEP and Tevatron data; the D6T [25] tune, which uses virtuality-ordered PS and is based on Tevatron data. The second generator used is PYTHIA8, which uses p_{T}-ordered PS, and the UE description is based on the multiple parton interaction (MPI) model of PYTHIA6 interleaved with initial and final state radiation. Four PYTHIA8 tunes are used: TUNE4C [26], TUNE2C, TUNE2M [26] [27], and TUNE4CX [27]. The third generator considered is HERWIG++ with tune TUNE23, where the PS is based on an angular-ordered shower. An eikonal multiple parton scattering model is used to simulate the UE. The last generator used is MADGRAPH, which uses matrix element (ME) calculations to generate events with two to four partons in different H_T bins and PYTHIA6-TUNEZ2 to generate the PS. The MLM matching procedure [28] is imposed to avoid double counting of jets between the ME and PS. In this matching algorithm, the minimum jet p_{T} threshold is set to be 10-40 GeV/c for different H_T bins.

5 Unfolding and Systematic Uncertainties

Jets at generator level are defined as the collection of generated final-state particles with the same kinematic criteria as the ones for the reconstructed data. The distribution of a variable obtained using generator-level information and detector-level information differs due to the finite energy and angular resolutions of the detector. In order to unfold the measured distributions from the detector level to the generator level, a response matrix is formed using simulated events. The D'Agostini method [29] is used to unfold the collision data, using the response matrix obtained from the fully simulated sample of events with PYTHIA6 generator and tune Z2. A regularized unfolding method based on singular value decomposition (SVD) of the response matrix [30] is also used as a consistency check.

Biases due to the choice of PYTHIA6 tune Z2 for the construction of the response matrix is tested by unfolding distributions using response matrices from PYTHIA6, PYTHIA8, and MADGRAPH samples. Although the results are consistent, small differences ($< 3\%$) are observed which are taken as a systematic uncertainty. Another source of systematic uncertainty in the unfolding procedure is the choice of the unfolding method. The difference between the two unfolding methods - D'Agostini and SVD - is less than 5% for the $T_{\perp,\mathcal{C}}$ distribution. It can be as high as 20% for the event shape distributions, which require more than three jets in the event mainly due to the smaller number of events in lower ranges of $p_{T,1}$. It can be as high as 20% in a few bins in other distributions, which require more than three jets in the event and these are mainly due to smaller number of events in lower ranges of $p_{T,1}$.

Another source of systematic uncertainty is due to the estimation of energy and angular resolution of jets [14]. The jet resolution effect is found to be less than 2% in most of the cases, but can be as high as 5%, and the jet energy scale effect is 3% or less. The statistical error arising from simulated event statistics does not exceed 2% in most cases, and never exceeds the statistical error of the data. The effect on these event shape variables from varying within uncertainties the proton collision pileup model was found to be negligible.

6 Results

Normalized (integrated area of the histogram is equal to unity) unfolded distributions of $\tau_{\perp,C}$, $B_{T,\mathcal{C}}$ and jet mass (both $\rho_{Tot,\mathcal{C}}$ and $\rho^{T}_{Tot,\mathcal{C}}$), along with the predictions from the different MC models considered, are presented in Figures 1 - 5. In Figure 6 the same comparison is made for $y_{23,\mathcal{C}}$.

The error bars around the data points represent the statistical uncertainties and the shaded yellow bands represent the sum in quadrature of statistical and systematic uncertainties. The ratio between the theory predictions and the data are shown in the lower plots, with the yellow bands representing the sum in quadrature of the systematic and statistical uncertainties, excluding the statistical error of the simulation.

The transverse thrust is insensitive to the longitudinal component of the particles' momenta, and is insensitive to modeling of MPI and color connection between soft scatters and beam remnants. It shows an agreement between data and predictions at the 5-10% level for all p_{T} bins, except at the highest $\tau_{\perp,\mathcal{C}}$. The agreement seen between data and predictions for this variable is better than the rest of the event shape variables, which are more sensitive to MPI and color connection effects. The $\tau_{\perp,\mathcal{C}}$ distributions reveal also that the predictions for the lower p_{T} bin, from PYTHIA8, HERWIG++, MADGRAPH and PYTHIA6(with tune D6T) are closer to data than the ones from PYTHIA6 with tune Z2 and PERUGIA-P0, indicating that the p_{T}-ordered PS

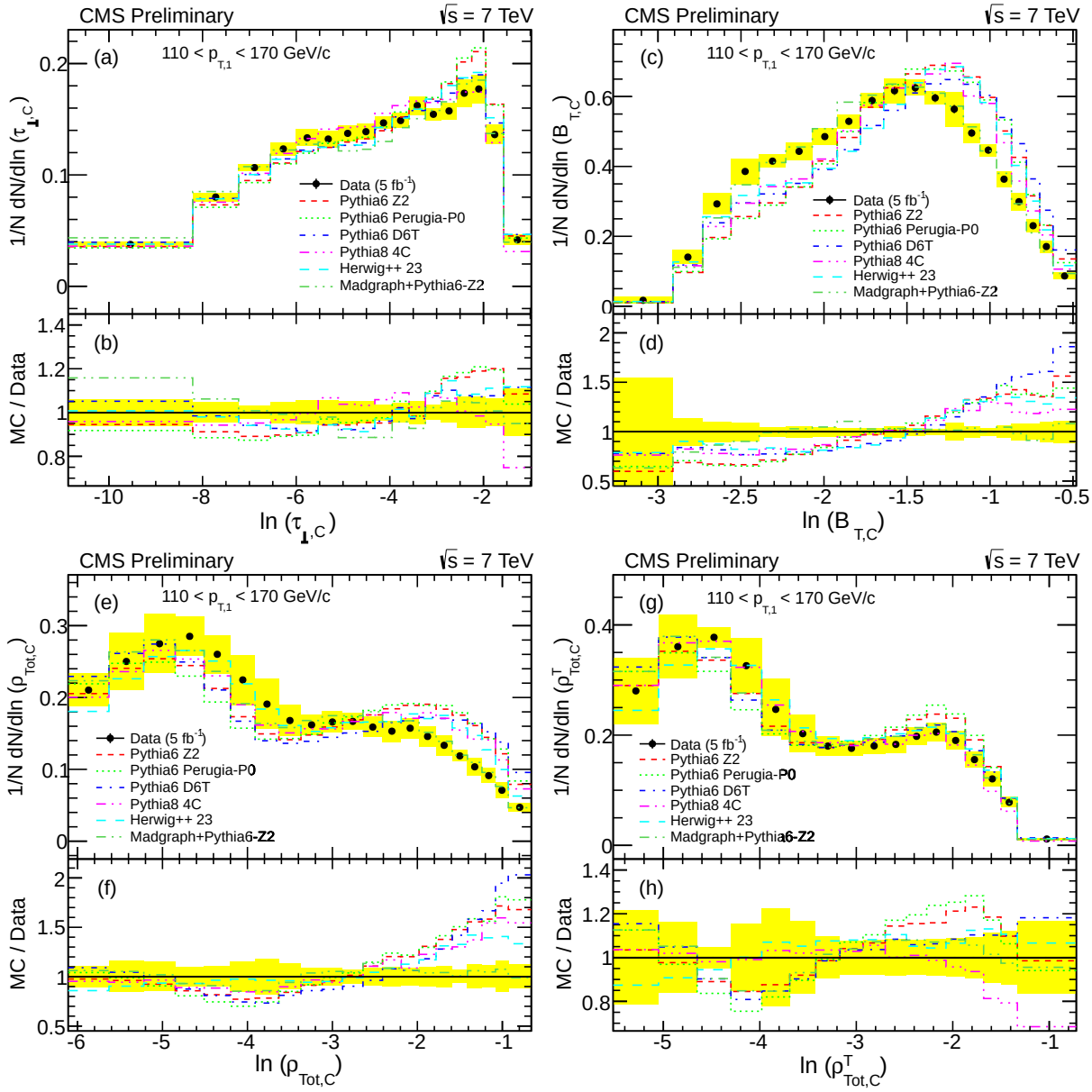

Figure 1: Comparison between data and various Monte Carlo models, in events with $110 < p_{\mathrm{T}} < 170$ GeV/c for the leading jet: (a) transverse thrust, (c) jet broadening spectra, (e) total jet mass, (g) total transverse jet mass, and (b,d,f,h) the ratios of MC samples with respect to data of the corresponding variables.

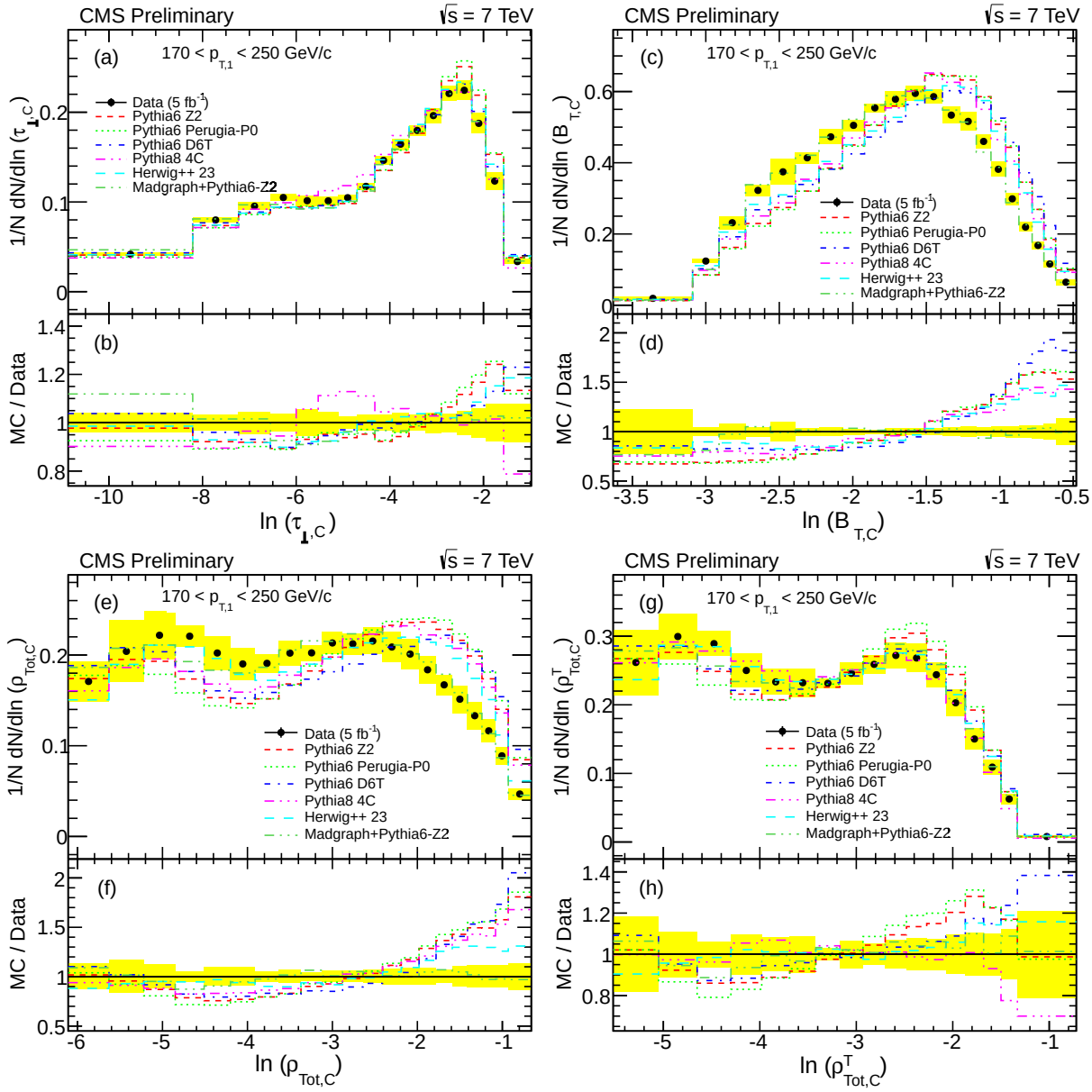

Figure 2: Comparison between data and various Monte Carlo models, in events with $170 < p_{\mathrm{T}} < 250$ GeV/c for the leading jet: (a) transverse thrust, (c) jet broadening spectra, (e) total jet mass, (g) total transverse jet mass, and (b,d,f,h) the ratios of MC samples with respect to data of the corresponding variables.

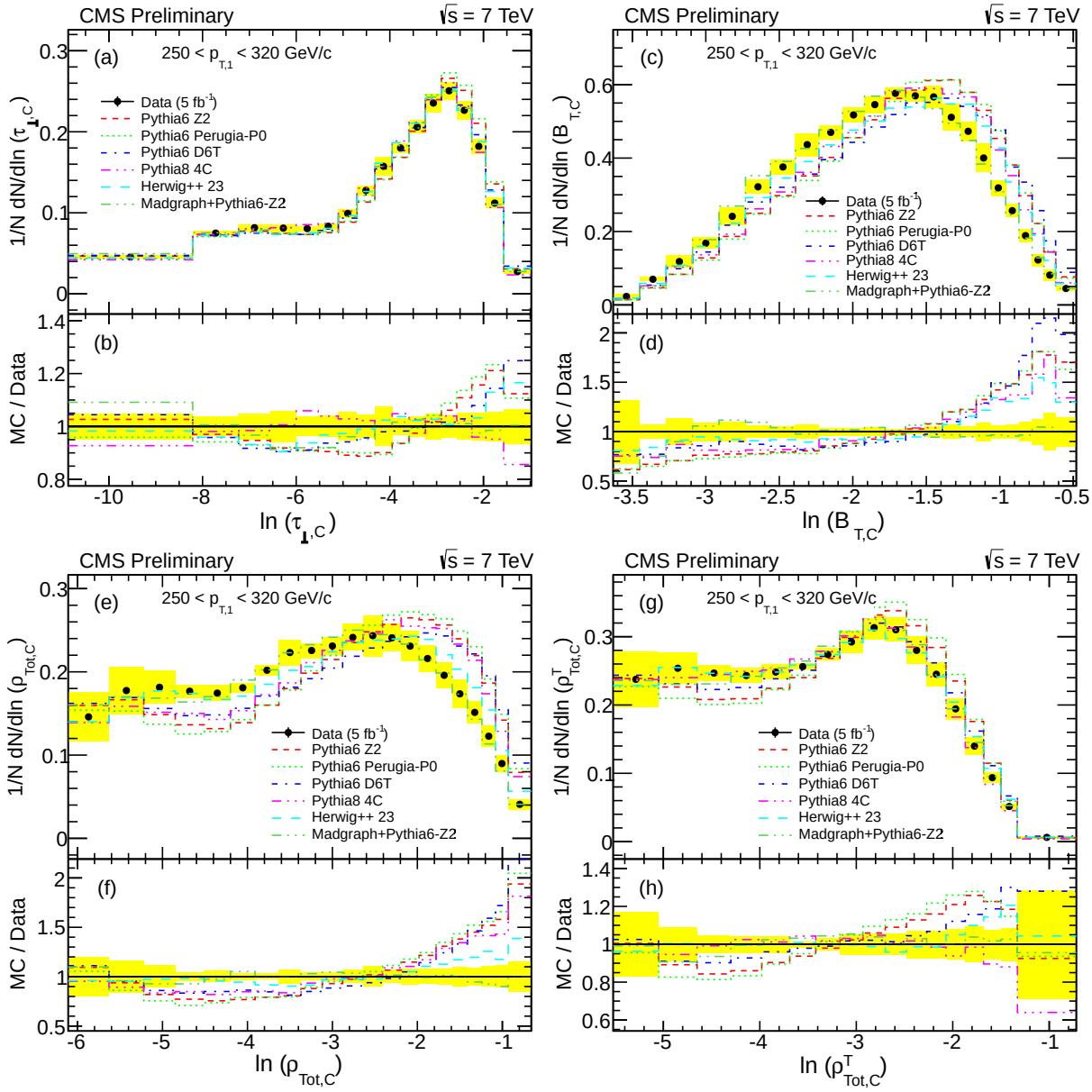

Figure 3: Comparison between data and various Monte Carlo models, in events with $250 < p_{\mathrm{T}} < 320$ GeV/c for the leading jet: (a) transverse thrust, (c) jet broadening spectra, (e) total jet mass, (g) total transverse jet mass, and (b,d,f,h) the ratios of MC samples with respect to data of the corresponding variables.

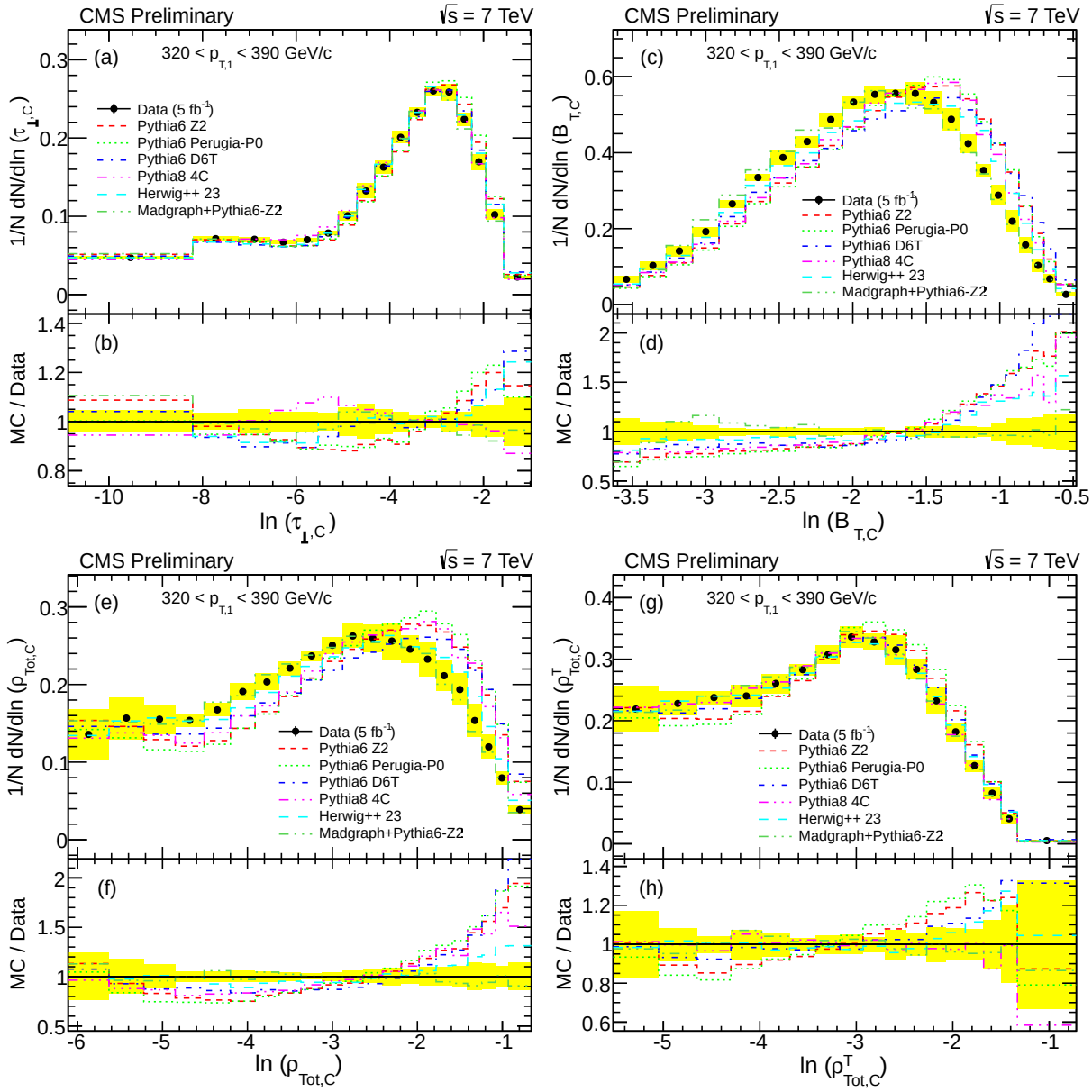

Figure 4: Comparison between data and various Monte Carlo models, in events with $320 < p_{\mathrm{T}} < 390$ GeV/c for the leading jet: (a) transverse thrust, (c) jet broadening spectra, (e) total jet mass, (g) total transverse jet mass, and (b,d,f,h) ratios of MC samples with respect to data of the corresponding variables.

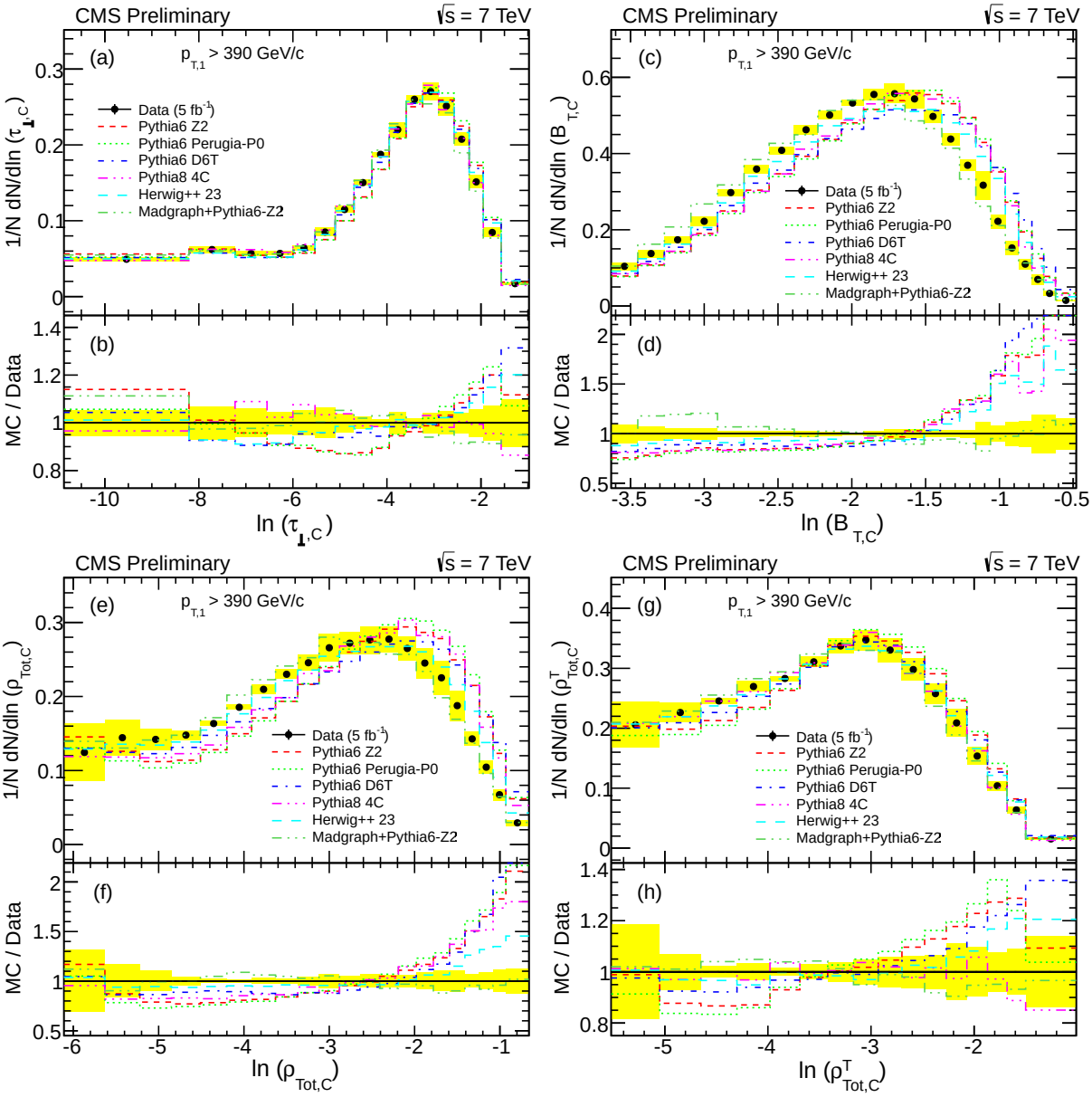

Figure 5: Comparison between data and various Monte Carlo models, in events with $p_T > 390$ GeV/c for the leading jet: (a) transverse thrust, (c) jet broadening spectra, (e) total jet mass, (g) total transverse jet mass, and (b,d,f,h) ratios of MC samples with respect to data of the corresponding variables.

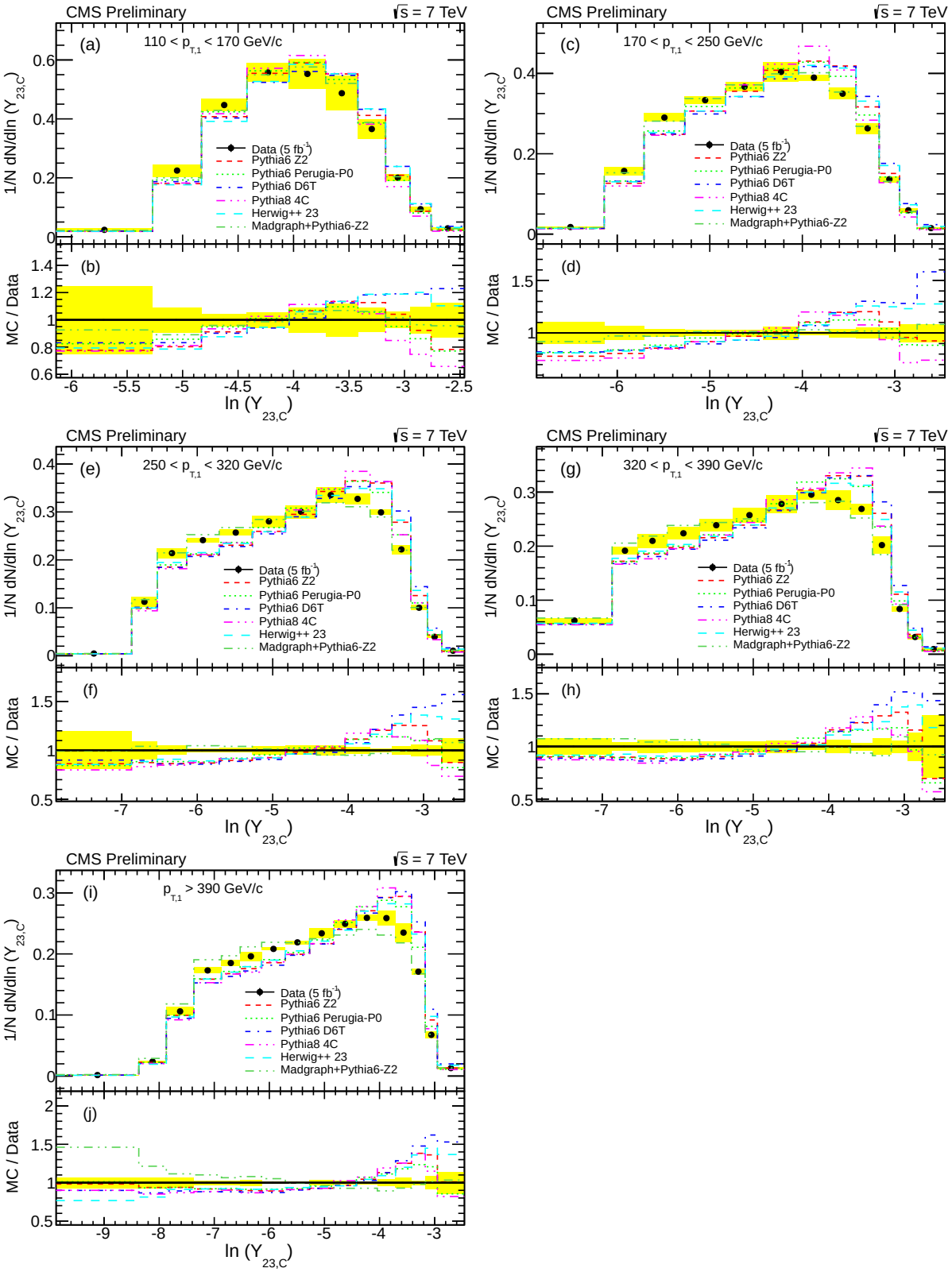

Figure 6: Comparison between data and various Monte Carlo models of the three jet resolution parameter, in events with (a) $110 < p_{\mathrm{T}} < 170$ GeV/c, (c) $170 < p_{\mathrm{T}} < 250$ GeV/c, (e) $250 < p_{\mathrm{T}} < 320$ GeV/c, (g) $320 < p_{\mathrm{T}} < 390$ GeV/c and (i) $p_{\mathrm{T}} > 390$ GeV/c for the leading jet. (b,d,f,g,j) ratios of MC samples with respect to the data in each momentum range.

in PYTHIA6 models is not able to reproduce the transverse event structure within the measured precision.

Jet broadening, $B_{T,\mathcal{C}}$ is insensitive to the contribution of the UE and hadronization. Hence, precise modeling of the ME and PS is crucial in order to predict the correct distributions. This is expected to be more adequate in the MADGRAPH generator, as it is based on ME for multi-parton final states, unlike the event generators PYTHIA and HERWIG++, which work best for $2\rightarrow2$ final states. In addition, jet broadening is sensitive to color coherence effects, hence there is better agreement with the current version of HERWIG++ which uses an improved color connection model [31]. In general, the agreement of this event shape variable with predictions is poor, except for the MADGRAPH and HERWIG++ generators for the reasons discussed above. The same arguments are also applicable for the total jet mass and the third-jet resolution parameter.

In the case of total jet mass ($\rho_{Tot,\mathcal{C}}$), the comparison of data with predictions shows nearly the same behavior as for the jet broadening. However, this variable is more sensitive to (initial-state) forward radiation than the jet broadening [2]. By comparing the distributions of the total jet mass and the total jet broadening, it is observed that this radiation effect is adequately introduced.

The transverse jet mass($\rho^{T}_{Tot,\mathcal{C}}$) distributions show agreement between data and predictions to within $\pm$ 20%, which is better than the one seen in total jet mass ($\rho_{Tot,\mathcal{C}}$). This is expected since transverse jet mass, like $\tau_{\perp,\mathcal{C}}$, is less sensitive to longitudinal event flow [2], and color connection effects. It is observed also that the PYTHIA6-D6T tune shows better agreement with data than the other tunes of PYTHIA6.

The third-jet resolution parameter ($y_{23,\mathcal{C}}$) distributions are shown in Figure 6 for the five different p_{T} bins. In the first p_{T} bin (110-170 GeV/c) the disagreement between data and theory is less than that of higher p_{T} bins. The same behavior is also observed for the total mass ($\rho_{Tot,\mathcal{C}}$). A possible source of this behavior is the large ISR effects for events with large p_{T} which are not properly accounted for by the generators considered except perhaps MADGRAPH.

Similar comparisons are performed using different jet clustering algorithms: anti-k_{T} with a distance parameter R = 0.7, k_{T} with a distance parameter R = 0.4 and energy deposits in the calorimeters only, and in all cases the results are similar and in agreement with each other.

The effect due to the choice of a particular parton distribution function (PDF) in the prediction of the distributions of event shape variables is estimated using the MSTW2008lo68cl PDF set [32, 33] and varying its parameters by one sigma, and is found to be negligible.

7 Summary

An extended set of event shape variables in multi-jet events: $T_{\perp,\mathcal{C}}$, $B_{T,\mathcal{C}}$, $\rho_{Tot,\mathcal{C}}$, $\rho^{T}_{Tot,\mathcal{C}}$, and $y_{23,\mathcal{C}}$, have been studied in detail and compared to simulated events using several different event generators. For the central thrust, all generators show an overall agreement with data to within 10%, with PYTHIA8 and HERWIG++ exhibiting a better agreement than the others. Variables which are sensitive to longitudinal energy flow in the event show a larger disagreement between data and theory, with the predictions of PYTHIA6 showing the worst agreement. The predictions of the virtual-ordered PS generator PYTHIA6 tune D6T show better agreement with data for the event shape variables that make use only of the jet p_{T}, but has worse worse agreement for $y_{23,\mathcal{C}}$ compared to other tunes of PYTHIA6. The predictions from MADGRAPH agree well with the data. Modeling of color connection between soft scatters and beam remnants, ISR, and FSR are the major sources of the discrepancies between the data and the various

QCD event generators.

References

[1] A. Banfi, G. P. Salam, and G. Zanderighi, "Resummed event shapes at hadron - hadron colliders", *JHEP* **0408** (2004) 062, doi:10.1088/1126-6708/2004/08/062, arXiv:hep-ph/0407287.

[2] A. Banfi, G. P. Salam, and G. Zanderighi, "Phenomenology of event shapes at hadron colliders", *JHEP* **1006** (2010) 038, doi:10.1007/JHEP06(2010)038, arXiv:1001.4082.

[3] M. Dasgupta and G. P. Salam, "Event shapes in e+ e- annihilation and deep inelastic scattering", *J.Phys.* **G30** (2004) R143, doi:10.1088/0954-3899/30/5/R01, arXiv:hep-ph/0312283.

[4] H1 Collaboration, "Measurement of event shape variables in deep-inelastic scattering at HERA", *Eur.Phys.J.* **C46** (2006) 343, doi:10.1140/epjc/s2006-02493-x, arXiv:hep-ex/0512014.

[5] L3 Collaboration, "Study of hadronic event shape in flavour tagged events in e+ e- annihilation at $\sqrt{s}$ = 197-GeV", *PMC Phys.* **A2** (2008) 6, doi:10.1186/1754-0410-2-6, arXiv:0907.2658.

[6] CDF Collaboration, "Measurement of Event Shapes in Proton-Antiproton Collisions at Center-of-Mass Energy 1.96 TeV", *Phys.Rev.* **D83** (2011) 112007, doi:10.1103/PhysRevD.83.112007, arXiv:1103.5143.

[7] T. Sjostrand, S. Mrenna, and P. Z. Skands, "PYTHIA 6.4 Physics and Manual", *JHEP* **0605** (2006) 026, doi:10.1088/1126-6708/2006/05/026, arXiv:hep-ph/0603175.

[8] CMS Collaboration, "First Measurement of Hadronic Event Shapes in pp Collisions at $\sqrt{s} = 7$ TeV", *Phys.Lett.* **B699** (2011) 48, doi:10.1016/j.physletb.2011.03.060, arXiv:1102.0068.

[9] ATLAS Collaboration, "Measurement of event shapes at large momentum transfer with the ATLAS detector in pp collisions at $\sqrt{s} = 7$ TeV", *Eur.Phys.J.* **C72** (2012) 2211, doi:10.1140/epjc/s10052-012-2211-y, arXiv:1206.2135.

[10] CMS Collaboration, "Event shapes and azimuthal correlations in Z + jets events in pp collisions at $\sqrt{s} = 7$ TeV", *Phys.Lett.* **B722** (2013) 238, doi:10.1016/j.physletb.2013.04.025, arXiv:1301.1646.

[11] CMS Collaboration, "The CMS experiment at the CERN LHC", *JINST* **3** (2008) S08004, doi:10.1088/1748-0221/3/08/S08004.

[12] "Commissioning of the Particle-flow Event Reconstruction with the first LHC collisions recorded in the CMS detector", Technical Report CMS-PAS-PFT-10-001, 2010.

[13] "Commissioning of the Particle-Flow reconstruction in Minimum-Bias and Jet Events from pp Collisions at 7 TeV", Technical Report CMS-PAS-PFT-10-002, CERN, Geneva, (2010).

[14] CMS Collaboration, "Determination of Jet Energy Calibration and Transverse Momentum Resolution in CMS", *JINST* **6** (2011) P11002, doi:10.1088/1748-0221/6/11/P11002, arXiv:1107.4277.

[15] M. Cacciari, G. P. Salam, and G. Soyez, "The Anti-k(t) jet clustering algorithm", *JHEP* **0804** (2008) 063, doi:10.1088/1126-6708/2008/04/063, arXiv:0802.1189.

[16] M. Cacciari, G. P. Salam, and G. Soyez, "FastJet User Manual", *Eur.Phys.J.* **C72** (2012) 1896, doi:10.1140/epjc/s10052-012-1896-2, arXiv:1111.6097.

[17] S. Catani, Y. L. Dokshitzer, M. Seymour, and B. Webber, "Longitudinally invariant K_t clustering algorithms for hadron hadron collisions", *Nucl.Phys.* **B406** (1993) 187, doi:10.1016/0550-3213(93)90166-M.

[18] S. D. Ellis and D. E. Soper, "Successive combination jet algorithm for hadron collisions", *Phys.Rev.* **D48** (1993) 3160, doi:10.1103/PhysRevD.48.3160, arXiv:hep-ph/9305266.

[19] T. Sjostrand, S. Mrenna, and P. Z. Skands, "A Brief Introduction to PYTHIA 8.1", *Comput.Phys.Commun.* **178** (2008) 852, doi:10.1016/j.cpc.2008.01.036, arXiv:0710.3820.

[20] M. Bahr et al., "Herwig++ Physics and Manual", *Eur.Phys.J.* **C58** (2008) 639, doi:10.1140/epjc/s10052-008-0798-9, arXiv:0803.0883.

[21] J. Alwall et al., "MadGraph 5 : Going Beyond", *JHEP* **1106** (2011) 128, doi:10.1007/JHEP06(2011)128, arXiv:1106.0522.

[22] GEANT4 Collaboration, "GEANT4: A Simulation toolkit", *Nucl.Instrum.Meth.* **A506** (2003) 250, doi:10.1016/S0168-9002(03)01368-8.

[23] R. Field, "Min-Bias and the Underlying Event at the LHC", *Acta Phys.Polon.* **B42** (2011) 2631, doi:10.5506/APhysPolB.42.2631, arXiv:1110.5530.

[24] P. Z. Skands, "Tuning Monte Carlo Generators: The Perugia Tunes", *Phys.Rev.* **D82** (2010) 074018, doi:10.1103/PhysRevD.82.074018, arXiv:1005.3457.

[25] R. Field, "Physics at the Tevatron", *Acta Phys.Polon.* **B39** (2008) 2611.

[26] R. Corke and T. Sjostrand, "Interleaved Parton Showers and Tuning Prospects", *JHEP* **1103** (2011) 032, doi:10.1007/JHEP03(2011)032, arXiv:1011.1759.

[27] R. Corke and T. Sjostrand, "Multiparton Interactions with an x-dependent Proton Size", *JHEP* **1105** (2011) 009, doi:10.1007/JHEP05(2011)009, arXiv:1101.5953.

[28] S. Mrenna and P. Richardson, "Matching matrix elements and parton showers with HERWIG and PYTHIA", *JHEP* **0405** (2004) 040, doi:10.1088/1126-6708/2004/05/040, arXiv:hep-ph/0312274.

[29] G. D'Agostini, "A Multidimensional unfolding method based on Bayes' theorem", *Nucl.Instrum.Meth.* **A362** (1995) 487, doi:10.1016/0168-9002(95)00274-X.

[30] A. Hocker and V. Kartvelishvili, "SVD approach to data unfolding", *Nucl.Instrum.Meth.* **A372** (1996) 469, doi:10.1016/0168-9002(95)01478-0, arXiv:hep-ph/9509307.

[31] "Measurement of color coherence effects in pp collisions at $\sqrt{s}$ = 7 TeV", Technical Report CMS-PAS-SMP-12-010, 2013.

[32] A. Martin, W. Stirling, R. Thorne, and G. Watt, "Parton distributions for the LHC", *Eur.Phys.J.* **C63** (2009) 189, doi:10.1140/epjc/s10052-009-1072-5, arXiv:0901.0002.

[33] A. Martin, W. Stirling, R. Thorne, and G. Watt, "Uncertainties on alpha(S) in global PDF analyses and implications for predicted hadronic cross sections", *Eur.Phys.J.* **C64** (2009) 653, doi:10.1140/epjc/s10052-009-1164-2, arXiv:0905.3531.